University of Groningen

Testing Verlinde's emergent gravity in early-type galaxies

Tortora, C.; Koopmans, L. V. E.; Napolitano, N. R.; Valentijn, E. A.

IMPORTANT NOTE: You are advised to consult the publisher's version (publisher's PDF) if you wish to cite from it. Please check the document version below.

Document Version
Publisher's PDF, also known as Version of record

[Link to publication in University of Groningen/UMCG research database](#)

Testing Verlinde's emergent gravity in early-type galaxies

C. Tortora,[1]⋆ L. V. E. Koopmans,[1] N. R. Napolitano[2] and E. A. Valentijn[1]

[1]*Kapteyn Astronomical Institute, University of Groningen, PO Box 800, NL-9700 AV Groningen, the Netherlands*
[2]*INAF – Osservatorio Astronomico di Capodimonte, Salita Moiariello, 16, I-80131 Napoli, Italy*

ABSTRACT

Emergent Gravity (EG) has been proposed to resolve the missing mass problem in galaxies, replacing the potential of dark matter (DM) by the effect of the entropy displacement of dark energy by baryonic matter. This apparent DM depends only on the baryonic mass distribution and the present-day value of the Hubble parameter. In this paper we test the EG proposition, formalized by Verlinde for a spherical and isolated mass distribution using the central dynamics (Sloan Digital Sky Survey velocity dispersion, σ) and the K-band light distribution in a sample of 4032 massive ($M_\star \gtrsim 10^{10}\,\mathrm{M_\odot}$) and local early-type galaxies (ETGs) from the SPIDER datasample. Our results remain unaltered if we consider the sample of 750 roundest field galaxies. Using these observations we derive the predictions by EG for the stellar mass-to-light ratio (M/L) and the initial mass function (IMF). We demonstrate that, consistently with a classical Newtonian framework with a DM halo component or alternative theories of gravity as MOdified Newtonian Dynamics (MOND), the central dynamics can be fitted if the IMF is assumed non-universal and systematically changing with σ. For the case of EG, we find lower, but still acceptable, stellar M/L if compared with the DM-based Navarro, Frenk & White (NFW) model and with MOND, but pretty similar to adiabatically contracted DM haloes and with expectations from spectral gravity-sensitive features. If the strain caused by the entropy displacement would be not maximal, as adopted in the current formulation, then the dynamics of ETGs could be reproduced with larger M/L.

Key words: galaxies: elliptical and lenticular, cD – galaxies: evolution – galaxies: general – galaxies: structure – dark matter.

1 INTRODUCTION

Dark matter (DM) is one of the biggest puzzles in the modern astrophysics and cosmology. This unseen mass component is thought to dominate the mass density of galaxies and clusters of galaxies in the Universe. It is essential to explain the high orbital velocities of gas and stars in the outer regions of spiral galaxies (Bosma 1978) and leaves its imprint at cosmological scales (e.g. Komatsu et al. 2011). DM is elusive, interacting very weakly with visible matter and has not been yet detected by any experiment. Thus, alternative ways to solve the missing mass problem have been suggested [e.g. MOdified Newtonian Dynamics (MOND), Milgrom 1983a,b], since it could be related to our poor understanding of gravity at the galactic and cluster scales. However, all kinds of approaches to solve the missing mass problem need to properly account for the stellar and gas content in galaxies and clusters. The first step in relating DM to visible matter of stars in the centres of galaxies (we neglect the contribution of gas in this paper) is the appreciation of the effective overall stellar mass-to-light ratio (M/L) of stellar populations, which today is still considered to be ill-constrained. In particular, the uncertainties on the number of low-mass stars can induce a change in the M/L of stars of about a factor 2 (e.g. Tortora et al. 2009). The distribution of stars in a galaxy, and thus the ratio between low- and high-mass stars, is described by the so called stellar initial mass function (IMF). Most of the studies of resolved stellar populations are obviously only possible in the Milky Way, where IMF was originally characterized as a power-law mass-distribution, dN/d$M \propto M^{-\alpha}$, with $\alpha \sim 2.35$ (Salpeter 1955), and subsequently refined to flatten at lower masses ($M \lesssim 0.5\,\mathrm{M_\odot}$; Kroupa 2001; Chabrier 2003). Chabrier- or Kroupa-like IMFs have been usually adopted in most types of galaxies, environments and redshifts. Recently, this hypothesis has been questioned by different lines of observational evidence (Treu et al. 2010; van Dokkum & Conroy 2010; Thomas et al. 2011; Conroy & van Dokkum 2012; Cappellari et al. 2012, 2013; Spiniello et al. 2012; Wegner et al. 2012; Barnabè et al. 2013; Dutton et al. 2013; Ferreras et al. 2013; Goudfrooij & Kruijssen 2013; La Barbera et al. 2013; Tortora, Romanowsky & Napolitano 2013; Weidner et al. 2013; Goudfrooij & Kruijssen 2014; McDermid et al. 2014; Tortora et al. 2014a,c; Shu et al. 2015; Martín-Navarro et al. 2015; Spiniello

et al. 2015; Lyubenova et al. 2016; Tortora, La Barbera & Napolitano 2016; Corsini et al. 2017; Li et al. 2017; Sonnenfeld, Nipoti & Treu 2017). In the current analysis we will express our results in terms of stellar M/L and the associated IMF, discussing whether these are realistic within different gravity frameworks.

As mentioned before, one of the alternatives to DM is the MOND by Milgrom (1983a,b), which proposes that the missing mass problem in galaxies could be resolved by a modification of Newton's law in the extremely low-acceleration regime. Newton's second law of dynamics becomes $F = mg$, where the acceleration g is related to the Newtonian one by $g\,\mu(g/a_0) = g_N$. Here, $a_0 \sim cH_0$ (where c is the speed of light and H_0 the Hubble constant) and $\mu(x)$ is the *interpolating function*, with the limiting behaviours $\mu(x \gg 1) = 1$ and $\mu(x \ll 1) = x$. It has been shown to reproduce flat rotation curves of spiral galaxies without the need for DM, and naturally predicting the observed relation between galaxy rotation and luminosity (Tully & Fisher 1977; Sanders & McGaugh 2002) or baryonic mass (McGaugh 2012). Only a few MOND analyses have been carried out on early-type galaxies (ETGs; e.g. Cardone et al. 2011; Ferreras et al. 2012; Milgrom 2012; Sanders 2014). Recently, Tortora et al. (2014c) have demonstrated that MOND is consistent with the central dynamics of ETGs if the stellar M/L are systematically larger in higher velocity dispersion (σ) galaxies, when compared with those calculated from stellar populations, assuming a universal stellar IMF. Thus, in MOND, the IMF is non-universal, suggesting that it is 'lighter' for low-σ galaxies, and 'heavier' for high velocity dispersions. This result is consistent with a plethora of independent studies using central dynamics (and/or gravitational lensing) with standard DM halo models or modelling spectral gravity-sensitive features (see above for a list of references).

A completely different proposal to supersede the presence of DM in the most massive virialized structures has been recently suggested (Verlinde 2011, 2017). This idea proposes that space–time and gravity are macroscopic concepts that arise from an underlying microscopic description in which these concepts have no meaning. We refer to this proposition as Emergent Gravity (EG) and use the formalism in Verlinde (2017). EG modifies gravity at scales set by the 'Hubble acceleration scale' a_0. Similarly to MOND, the gravitational force emerging in the EG framework exceeds that of General Relativity (GR) on supergalactic and cluster scales. However, the underlying physical modelling in EG is rather different. Unlike MOND and DM-based models, the (apparent) DM distribution only depends on the baryonic mass distribution $M_b(r)$ and H_0. But, most importantly, it depends on the radial mass density gradients, which could provide the ultimate tool for testing and comparing the validity of EG. Note that the formalism for EG has currently only been derived for spherical symmetric baryonic mass distributions, and any test should account for these still very first and simplified predictions.

Some papers have recently tested this new proposition on different scales using weak gravitational lensing signal (Brouwer et al. 2017), dynamics of dwarf spheroidal satellites of the Milky Way (Diez-Tejedor, Gonzalez-Morales & Niz 2016), dwarf galaxies (Pardo 2017), the radial acceleration relation in spiral galaxies (Lelli, McGaugh & Schombert 2017), galaxy rotation curves and Solar system planets' perihelia (Hees, Famaey & Bertone 2017), X-ray galaxy clusters (Ettori et al. 2017), lensing and X-ray in clusters (Nieuwenhuizen 2017) finding contrasting results. Milgrom & Sanders (2016) have highlighted some limits in Verlinde's EG proposition.

In this paper, we will test the EG predictions in the central regions of massive (with stellar masses $M_\star \gtrsim 10^{10}\,M_\odot$) and local (with redshifts $0.05 < z < 0.095$) ETGs from the SPIDER survey (La Barbera et al. 2010a). We fix the Hubble parameter and allow the only free parameter of the model, i.e. the stellar M/L, to vary, evaluating our results in terms of the IMF. Then, we compare the EG results with MOND, DM haloes and with findings from gravity-sensitive spectral features. We will also analyse how the Hubble constant value, and thus the acceleration scale, impact our results, discussing how the strain caused by the entropy displacement can be constrained. The paper is organized as follows. In Section 2 we introduce the EG proposition, discussing hypothesis and approximations. Standard models for DM haloes and MOND theory are described in Section 3. The data sample is presented in Section 4. In Section 5 we will discuss the results of our dynamical analysis, and finally Section 6 is devoted to discussion and conclusions.

2 EMERGENT GRAVITY

EG refers to the idea that space–time and gravity are macroscopic effects arising from underlying microscopic physical phenomena. In many fields of the physics, macroscopic phenomena 'emerge' from microscopic processes, for example thermodynamics arising from microscopic states of matter or the Van der Waals force emerging from non-relativistic quantum electrodynamics. Examples are found in different physical environments and thus it is not inconceivable that the nature of gravity could be the macroscopic and cumulative effects of some unknown microscopic physics. Moreover, this would not be surprising considering that classical GR already has signatures which link it to thermodynamics, e.g. black hole thermodynamics. These ideas are not new and different approaches have been followed to describe the emergent gravity (e.g. Sindoni 2012).

In the context of EG, Jacobson (1995) has shown how Einstein equations can be recovered from the black hole entropy and the standard concepts of heat, entropy and temperature in thermodynamics. The idea that gravity is an entropic force was further explored by Padmanabhan (2010) and Verlinde (2011). They suggested that an 'area law' scaling of gravitational entropy, as opposed to the usual volume scaling, is essential to derive Einstein's laws of gravity. Motivated by all these ideas, Verlinde (2017) has used these thermodynamic concepts to suggest a possible alternative explanation for DM. He suggests that the quasi-de Sitter space–time, which would be a fair approximation of the present Universe, dominated by dark energy, can be obtained from a system of microstates which are coherently excited above the true vacuum. This ground state corresponds to an anti-de Sitter space–time filled by a negative cosmological constant and emerges from microstates which are entangled. Thus, Verlinde (2017) uses the theory of elasticity (Padmanabhan 2004) and has suggested that in addition to the area law, a volume entanglement of entropy can be postulated. The stress between the area law in Verlinde (2011) and the volume law in Verlinde (2017) manifests itself in spherical galaxies as an apparent DM on scales set by the 'Hubble acceleration scale' $a_0 = cH_0$, where c is the speed of light and H_0 the present-day Hubble parameter. By studying the dynamics of galaxies and clusters, it is possible to test the evidence for this postulate.

Thus, according to Verlinde (2017), there exists an extra gravitational effect, in addition to the classical GR contribution of $M_b(r)$ to the gravitational potential. This excess in the gravity emerges due to the volume law contribution to the entropy that is associated with the dark energy content of our universe. In a universe without matter, the total entropy of the dark energy would be maximal, as it would be homogeneously distributed over the microstates. In our

Universe, on the other hand, its baryonic mass distribution $M_b(r)$ reduces the entropy content of the universe. This removal of entropy due to matter produces an elastic response of the underlying microscopic system, which can be observed on galactic and supergalactic scales as an additional gravitational force. The difference with GR is that this excess gravity does not come from the existence of DM. However, the excess mass in Verlinde's proposal can still be described by an *apparent* DM distribution $M_{DM}(r)$.

2.1 Formulation

We start with some qualitative arguments. A system with a static, spherically symmetric and isolated baryonic mass distribution is analysed (see Verlinde 2017 for further details). We consider a spherical region with boundary area $A(r) = 4\pi r^2$, which contains a mass M near its centre. The surface mass density $\Sigma_M(r)$ is defined as the ratio of the mass M and the area $A(r)$. Empirically, the directly observed gravitational phenomena attributed to DM is thought to occur when the surface mass density falls below a universal value determined by the acceleration scale a_0 (e.g. Milgrom 1983a). This condition could be written as $\Sigma_M(r) < a_0/(8\pi G)$, where $a_0 = cH_0$. This inequality is made more clear if written in terms of de Sitter entropy removed by adding the mass M, i.e. S_M, and the one related to dark energy, S_{DE}. In this regime, we assume the inequality $S_M < S_{DE}$ holds. The nature of gravity changes depending on whether matter removes all or just a fraction of the de Sitter entropy. In general, we can define the strain $\epsilon_M(r) \equiv S_M/S_{DE} = 8\pi G \Sigma M/a_0$. If $\epsilon_M(r) > 1$ the dynamics of stellar objects behaves as in a Newtonian framework, while if $\epsilon_M(r) < 1$, then we are in the regime of low surface mass density and low acceleration, i.e. in the 'dark gravity' regime. ϵ_M corresponds to the largest principle of the elastic medium strain. Thus, when only a part of the de Sitter entropy is removed by matter inclusion, the remaining entropy induces a non-negligible effect, leading to modifications of the normal gravitational laws in the Newtonian regime. This translates into an 'apparent' surface density produced by baryons, $\Sigma_{DM} = (a_0\epsilon_{DM})/(8\pi G)$. To determine these modifications, we would need to analyse the displacement of the entropy content, due to matter, applying the linear elasticity theory (Verlinde 2017).

The quantity of apparent DM can be obtained by estimating the elastic energy associated with the entropy displacement caused by $M_b(r)$. After some calculations, this leads to the following relation[1]:

$$\int_0^r \epsilon_{DM}^2(r')A(r')dr' \leq V_{M_b}(r),$$ (1)

where we integrate over the sphere with radius r and area $A(r)$. The strain $\epsilon_{DM}(r)$ caused by the entropy displacement is given, as defined previously, by

$$\epsilon_{DM}(r) = \frac{8\pi G}{cH_0} \frac{M_{DM}(r)}{A(r)},$$ (2)

Furthermore, $V_{M_b}(r)$ is the volume that would contain the amount of entropy that is removed by a mass M_b inside a sphere of radius r, if that volume were filled with the average entropy density of the universe

$$V_{M_b}(r) = \frac{8\pi G}{cH_0} \frac{M_b(r)\,r}{3}.$$ (3)

---

[1] We avoid to report the lengthy calculations made in Verlinde (2017). The reader can refer to that paper for further information.

Equation (1) deserves some attention because due to the inequality, observations can only put a lower bound on the M_{DM} and H_0, since a larger value can be accommodated by having a smaller elongation (or compression) of the elastic medium due to the baryonic mass inclusion. Throughout this paper, we assume that the largest principle strain $\epsilon_{DM}(r)$ takes its maximal value and the response of the medium is negligible outside the mass. These assumptions authorize us to adopt the equality in equation (1).

Thus, inserting the relations (2) and (3) into (1), and taking the derivative with respect to r on both sides of the equation, one arrives at the following relation:

$$M_{DM}(r) = r\sqrt{\frac{cH_0}{6G}}\sqrt{\frac{d\,(M_b(r)r)}{dr}}.$$ (4)

This is the apparent DM formula, which translates a baryonic mass distribution into an apparent DM distribution. As it emerges from equation (4), the EG formalism naturally provides the value of a characteristic acceleration scale, $a_{EG} \equiv cH_0/6$.

In our analyses, the mass from equation (4) is added to baryons and the resulting mass is converted into a velocity dispersion using the standard Jeans equations and treating the apparent DM in EG as a real mass component. These predicted velocity dispersions are subsequently compared with the observed velocity dispersions. We will discuss this procedure in more details in the following sections.

2.2 Caveats and assumptions

Currently equation (4) is the only specific prediction of the DM in the EG framework and we will use it in the rest of this paper, recognizing the following caveats and restrictions, which as a matter of fact also apply to various other recent papers on EG predictions (Diez-Tejedor et al. 2016; Brouwer et al. 2017; Ettori et al. 2017; Hees et al. 2017; Lelli et al. 2017; Nieuwenhuizen 2017; Pardo 2017). In particular, we will discuss: (a) the assumption of spherical symmetry and isolation of the mass distribution (Section 2.2.1); (b) the cosmological framework, motivating our assumptions about the present-day Hubble parameter (Section 2.2.2); (c) the limitations of the equality in equation (1) (Section 2.2.3); and finally (d) our assumption that the Jeans equations are the same as used in a Newtonian or MONDian framework (Section 2.2.4).

2.2.1 ETGs: spherically symmetric and isolated

The predictions of the excess mass in EG is currently only valid for static, spherically symmetric and isolated baryonic mass distributions. Therefore, one of the best test-bench for Verlinde's EG is represented by ETGs, which match these characteristics. As we will discuss, massive ETGs are among the best galaxy candidates, since many of them are approximatively spherically symmetric. ETGs contain most of the stellar mass of the universe and represent the final stage of galaxy evolution (Fukugita, Hogan & Peebles 1998). In a standard Λ cold dark matter (CDM) scenario, they are thought to be fossil records of the stellar and DM assembly through time. In this scenario, DM is dominant in the external regions, while the extremely complex physics of gas and stars are dominant in the central regions. ETGs exhibit a peaked surface brightness profile and historically have been considered to be well fitted by a de Vaucouleurs (1948) profile, in contrast to late-type systems which present more extended and shallow light distributions, which are described by exponential profiles. However, more detailed analyses show that their light distributions are well described by the Sérsic law (Ciotti 1991), with a shape parameter, n (Sérsic index), that

accounts for variations of the light profile shape among galaxies ($n = 4$ corresponds to a de Vaucouleurs 1948 profile). These steep profiles are also accompanied by the absence of disc and spiral arm structures and are thought to be the result of accretion (Hilz, Naab & Ostriker 2013; Tortora et al. 2014b, 2017).

ETG shapes are well described by an oblate or triaxial ellipsoid and when projected on the sky, they have small ellipticities, becoming rounder towards larger masses (Vulcani et al. 2011). However, also when a residual small ellipticity is present, as in most ETGs, the spherical approximation is far better than a similar assumption for spiral galaxies, which are characterized by a central bulge and a pronounced disc, which is far to be approximated by a sphere. The difference between spherical and disc geometry can induce corrections of the order of ∼20 per cent for spirals (Lelli et al. 2017).

Moreover, ETGs are found to live in all galaxy environments, from the field to groups and clusters of galaxies. From this point of view they are also good candidates to test Verlinde's proposal, which has produced an expression for the excess mass for an object only if it is sufficiently far from any other mass distribution and unaffected by recent or ongoing merging-events or close interactions.

2.2.2 Cosmological framework

In order to test EG predictions, we need to make some assumptions about the adopted cosmology, which enters in the distances and the evolution of the Hubble parameter in equation (4). Verlinde's arguments only hold in a static Newtonian approximation, allowing one to describe gravity phenomena on galactic and super-galactic scales, but they are not sufficient to include the evolution of the Universe. His EG proposal has been only developed in a de Sitter space–time, which relies on the approximation that our universe is entirely dominated by dark energy (in particular by a cosmological constant Λ) and that standard baryonic matter only leads to a small perturbation. Two main issues arise from these assumptions. First, in a de Sitter space–time, the Hubble parameter can be written as $H(z) = \mathcal{H}_0\sqrt{\Omega_\Lambda} \propto \sqrt{\Lambda}$, which means it is constant with time. This motivates the assumption about $H_0 = H(z=0) = H(z)$ adopted by Verlinde in equation (4). Another approximation is in the assumption that the dark energy is the dominant contributor to the energy density of the Universe. This is an incorrect approximation mainly at the early stages of the Universe, when the contribution of the dark energy is smaller compared with other energy contributors.

In a standard ΛCDM framework, the following formula holds $H(z) = \mathcal{H}_0\sqrt{\Omega_m(1+z)^3 + \Omega_\Lambda}$, and from the comparison with CMB spectrum it is found that the Universe is flat and thus $H(z=0) = \mathcal{H}_0$ (e.g. Komatsu et al. 2011). But this is obviously not true in a de Sitter space–time, where the Hubble parameter at $z = 0$ depends on the cosmological constant.

A de Sitter space–time is not a realistic model capable to fit the cosmological data, and in particular cannot fit the $H(z)$ inferred from standard cosmological data [e.g. redshift-distance relation in Type-Ia Supernoavae, Riess et al. 1998; cosmic microwave background (CMB) anisotropies, Komatsu et al. 2011; the baryon acoustic oscillation, BAO, peaks, Percival et al. 2010] nor observational $H(z)$ data using passive galaxies as 'cosmic chronometers' [observational Hubble parameter data (OHD), Jimenez et al. 2003; Zhang et al. 2014]. However, at low redshifts, the shape of $H(z)$ determined from observational probes are almost independent on the exact cosmological model adopted. This is true since various models are fitting the data producing local $H(z)$ values which are consistent with H_0 from ΛCDM cosmology within the measurement uncertainties (e.g. Carvalho et al. 2008; Zhang et al. 2014; Farooq et al. 2017). For the redshifts studied in this paper, i.e. $z < 0.1$, the cosmological evolution has a negligible effect on the distance measurements and on Verlinde's equations. Thus, we assume that observations at $z \sim 0$ can be reproduced by an effective ΛCDM model with $\Omega_m = 0.3$, $\Omega_\Lambda = 0.7$ and $H_0 = 75$ km s^{-1} Mpc^{-1}. Here we stay in line with all of the recent papers that have directly or indirectly adopted a background ΛCDM cosmology (Diez-Tejedor et al. 2016; Brouwer et al. 2017; Ettori et al. 2017; Hees et al. 2017; Lelli et al. 2017) to set the value of H_0 in equation (4) and the distances, and some of them investigated the impact of a varying a_0. Again in line with these papers, we will also discuss the case when a_0, and thus H_0, changes (e.g. Hees et al. 2017; Lelli et al. 2017).

2.2.3 Only a lower bound on DM distribution

Verlinde, as in all the recent literature which addressed his proposal, have assumed that the excess gravity generated from the elastic response and the related apparent DM distribution take their maximal value. This translates to an equality in equation (1). If we consider the inequality in Verlinde's formula, then a fixed amount of baryons will correspond a smaller M_{DM}. The strain would assume reasonably the largest value sufficiently close to the bulk of mass distribution, where the contribution of the apparent DM first becomes noticeable (Verlinde 2017). But, getting further out, or when other mass distributions come in, the inequality holds. Thus, in the central regions of ETGs this assumption would seem more reasonable, but it does remain arbitrary and needs to be tested. Thus, the relaxation of the equality in our assumption would provide some constraints on the entropy strain.

2.2.4 Jeans equations

We will interpret measured velocity dispersions in terms of gravity by applying the Jeans theorem and assume this is justified in an EG formalism. In this section we will motivate why this is the case. ETGs are self-gravitating systems of stars with random motions, which can be quantified by the velocity dispersion. In a standard Newtonian framework, the motions of stars in the gravitational potential are described by the Jeans equations, which are derived from the collisionless Boltzmann equation and relate the components of the velocity dispersion of the system (e.g. in polar coordinates, σ_r, σ_θ and σ_ϕ) to the gravitational potential $\phi(r)$, and thus to the mass distribution (Binney & Tremaine 1987). The radial Jeans equation is the relevant formula in this paper and gets a very simple expression if one assumes (a) a steady-state hydrodynamic equilibrium; (b) spherical symmetry; and (c) a single tangential velocity dispersion σ_t:

$$\frac{\mathrm{d}\left[j_\star(r)\sigma_r^2(r)\right]}{\mathrm{d}r} + 2\frac{\beta(r)}{r}j_\star(r)\sigma_r^2(r) = -j_\star(r)\frac{GM(r)}{r^2}, \qquad (5)$$

where $j_\star(r)$ and $M(r)$ are the deprojected light and total mass distribution, and $\beta = 1 - \sigma_t^2/\sigma_r^2$ is the anisotropy. This equation holds in the Newtonian case, but can be easily generalized to account for generic acceleration function $g(r)$, and in particular for MOND formalism, as[2]

$$\frac{\mathrm{d}\left[j_\star(r)\sigma_r^2(r)\right]}{\mathrm{d}r} + 2\frac{\beta(r)}{r}j_\star(r)\sigma_r^2(r) = -j_\star(r)g(r), \qquad (6)$$

which assumes the standard expression in equation (5) when $g(r) = GM(r)/r^2$.

---

[2] We notice that there is a typo on the right side of equation (2) in Tortora et al. (2014c).

We can use one of the previous two formulas, by just replacing $M_{DM}(r) + M_\star(r)$ in equation (5), or, using the MOND formalism, evaluating the centripetal acceleration associated with this apparent total mass in equation (6), consistently with the interpolating function provided in Hees et al. (2017). The radial velocity dispersion from the Jeans equations has to be first integrated along the line of sight and then projected within a finite aperture (rectangular or circular; Tortora et al. 2009). Then, this quantity can be compared to the observed aperture velocity dispersion, σ_{Ap}, to determine the stellar M/L and/or the present-day Hubble parameter, the only free parameters in equation (4).

We do not find any strong argument against a similar formalism in the Verlinde's framework, where the hypothesis and approximations discussed to obtain the radial Jeans equations seem to be satisfied. Thus, following Diez-Tejedor et al. (2016) we adopt the radial Jeans equation in equation (5), inserting the total mass, obtained summing up the baryonic and apparent DM mass derived from equation (4), i.e. $M(r) = M_\star(r) + M_{DM}(r)$, assuming for the stellar distribution a constant M/L profile. However, this assumption will need to be better analysed in the future.

3 NEWTONIAN AND MONDIAN FRAMEWORK

Here we will adopt some specific DM halo models and also MOND determining their best-fitting stellar M/Ls and comparing these results with those from EG. In the Newtonian framework, we adopt a two-component model (stars + DM). For the DM distribution we assume some DM halo models, fixing their parameters according to viable recipes, which we will discuss below. While, for the EG and MOND propositions, we use a constant M/L profile, with free stellar M/L, $\Upsilon_\star$, for the stellar distribution.

Results using these DM-based models have been presented in Tortora et al. (2013) and Tortora et al. (2014a). New results using MOND with SPIDER data set are presented here for the first time. In Tortora et al. (2014c) we tested MOND using a different datasample, but finding similar results. In the rest of this section, we provide details about all these models.

3.1 DM-based models

The DM profile from *N*-body simulations is well described by a double power law, commonly referred to as the NFW profile, parametrized by two parameters, the virial concentration index c_{vir} and the (total) virial mass M_{vir} (Navarro, Frenk & White 1996, 1997). We adopt NFW as the reference DM model, assuming (a) the correlation between M_{vir} and c_{vir} from *N*-body simulations based on WMAP5 cosmology (Macciò, Dutton & van den Bosch 2008); as well as (b) the M_{vir}–$M_\star$ correlation from abundance matching results in Moster et al. (2010), assuming a Chabrier IMF for $M_\star$. In this way, for each galaxy with a stellar mass $M_\star$, M_{vir} and c_{vir} are empirically set, and the DM profile is fully determined.

In order to explore the effect of a possible modification to the DM profile because of the interaction between gas and stars with DM, we also consider the case of an NFW profile with an adjustable degree of baryon-induced adiabatic contraction (AC; e.g. Blumenthal et al. 1986; Gnedin et al. 2004). AC is an approximate way to model the expected drag of dissipatively infalling stars on the surrounding DM particles producing a halo with a higher central DM density than in collisionless *N*-body simulations. Following Napolitano, Romanowsky & Tortora (2010) we adopt the Gnedin et al. (2004) prescription.

We have also explored how these results depend on the assumed M_{vir}–c_{vir} relation (Tortora et al. 2013, 2014a).

We have analysed the impact of the mass density law adopting a Burkert (1995) profile, which is the prototype of cored models, and has been shown to reproduce the DM profile of spirals and dwarf galaxies. The density and scale parameter of the Burkert profile (ρ_B and r_B, respectively) are assumed to follow the relation from Salucci & Burkert (2000), adjusted to match results at higher surface density, for two ETGs, by Memola, Salucci & Babić (2011). We have explored two cases in detail, where the scale radius is set to $r_B = 1$ and $20\,kpc$, respectively. We have shown in Tortora et al. (2014a) that the exact value of r_B has a negligible impact on the inferred stellar M/L values.

3.2 MOND-based models

MOND assumes that standard dynamics is not valid in the limit of low accelerations, such that the gravitational acceleration $g(r)$ differs from the Newtonian one $g_N(r) = GM_\star/r^2$. The MONDian $g(r)$ reduces to the Newtonian one at high accelerations. In the low-acceleration limit, i.e. deep in the MONDian regime, the acceleration is given by $(g/a_0)g = g_N$, where a_0 is the MOND acceleration constant. MOND predicts flat rotation curves in the external regions of spiral galaxies and naturally leads to the Tully & Fisher (1977) relation. The characteristic acceleration scale a_0 is a fundamental parameter of the theory (Milgrom 1983a). In this paper, we adopt the standard value of $a_0 = 1.2 \times 10^{-10}\,m\,s^{-2}$, as calibrated from spiral galaxy dynamics (Begeman, Broeils & Sanders 1991). This value is found to be of the same order of magnitude as the 'acceleration' associated with the Hubble constant, i.e. $\approx cH_0$, and to the cosmological constant Λ, $\approx c(\Lambda/3)^{1/2}$ (Milgrom 2001). If we use the definition provided in EG, i.e. $a_0 = a_{EG} \equiv cH_0/6$, then the value adopted for a_0 corresponds to $H_0 \approx 75\,km\,s^{-1}\,Mpc^{-1}$.

To connect the low- and high-acceleration regimes, the following expression is adopted:

$$g(r)\mu\left[\frac{g(r)}{a_0}\right] = g_N(r), \tag{7}$$

where $x = g(r)/a_0$ and $\mu(x)$ is an empirical 'interploating' function with the properties $\mu(x \gg 1) = 1$ and $\mu(x \ll 1) = x$. One recovers the Newtonian theory when $\mu(x) = 1$ and the deep MOND regime when $\mu(x) = x$. An alternative expression can be obtained making the substitution $\nu(y) = \mu(x)^{-1}$, where $y \equiv g_N/a_0$.

We adopt the following expressions:

(i) the first attempts to fit rotation curves adopted the interpolating function $\mu(x) = x/\sqrt{1 + x^2}$ (Milgrom 1983a; Sanders & McGaugh 2002);

(ii) later on another law has been suggested to provide a better description of some data, i.e. the 'simple' function $\mu(x) = x/(1 + x)$ (Famaey & Binney 2005; Angus 2008);

(iii) recently, using more than 2500 data points in a sample of 153 rotationally supported galaxies, McGaugh, Lelli & Schombert (2016) suggested the following expression $\nu(y) = (1 - \exp(-\sqrt{y}))^{-1}$.

A constant M/L profile with a free $\Upsilon_\star$ is adopted for the total mass distribution (see Tortora et al. 2014c for further details). To reduce the computation time, we follow the same binning procedure used in Tortora et al. (2013), constructing 'average' galaxies by dividing our sample into different σ_e-bins, for which we compute median values of all the stellar parameters (R_e, n, $M_\star$, R_{Ap}, σ_{Ap}). For each σ_e-bin and a given interpolation function, we solve the radial Jeans equation

equation (6) for the $\Upsilon_\star$ value matching the observed average σ_{Ap} in the bin.

4 DATA SAMPLE

In this section, we will describe the sample of galaxies used and their main properties that we use to test the DM, MOND and EG models.

4.1 SPIDER sample

The SPIDER survey has demonstrated to be very useful in the study of the luminous and DM distribution in the galaxy cores (Tortora et al. 2012, 2013, 2014a). It consists of a sample of 5080 bright ($M_r < -20$) ETGs, in the redshift range of $z = 0.05$–0.095, with optical and near-infrared (NIR) photometry available (*grizYJHK* bands) from the Sloan Digital Sky Survey (SDSS) DR6 and the UKIRT Infrared Deep Sky Survey-Large Area Survey DR3[3] (La Barbera et al. 2010a). Sérsic profile is fitted to the surface photometry using 2DPHOT (La Barbera et al. 2008). Thus, the effective radius R_e and Sérsic index n have been measured from *g* through *K* bands. SPIDER ETGs have central velocity dispersions, σ_{Ap}, measured in the circular aperture of the SDSS fibre ($R_{\mathrm{Ap}} = 1.5$ arcsec). The median ratio of the SDSS fibre to the *K*-band effective radius is $R_{\mathrm{Ap}}/R_e \sim 0.6$. The σ_e is the SDSS-fibre velocity dispersion, σ_{Ap}, corrected to an aperture of one R_e following Cappellari et al. (2006).

ETGs are defined as bulge-dominated systems (i.e. SDSS parameter *fracDev$_r$* > 0.8, which measures the fraction of galaxy light better fitted by a de Vaucouleurs, rather than an exponential law), with passive spectra within the SDSS fibres (SDSS attribute *eClass* < 0, where *eClass* indicates the spectral type of a galaxy based on a principal component analysis). See La Barbera et al. (2010a) for further details. For the present work, we rely on a subsample of 4032 SPIDER ETGs, with higher quality optical and NIR structural parameters, selected as in Tortora et al. (2012), with Sérsic fits having $\chi^2 < 2$ in all wavebands and uncertainty on $\log R_e < 0.5$ dex, as well as stellar masses $M_\star \gtrsim 10^{10}\,\mathrm{M_\odot}$ and velocity dispersions $\gtrsim 100\,\mathrm{km\,s^{-1}}$. For each galaxy, the stellar population-based M/L ratio, $\Upsilon_{\star\mathrm{Chab}}$, has been determined by fitting Bruzual & Charlot (2003) stellar population models to the multiband photometry, under the assumption of a Chabrier IMF (Swindle et al. 2011; Tortora et al. 2012).

All these galaxies reside on the red-sequence, with more than 99 per cent having $g - r \gtrsim 0.5$, within an aperture of 1 R_e, and a median $g - r = 0.88$. Stellar mass (Chabrier IMF-based) and aperture velocity dispersions for the sample are in the ranges $\sim(0.1$–$3) \times 10^{11}\,\mathrm{M_\odot}$ and $\sim(100$–$250)\,\mathrm{km\,s^{-1}}$, with medians of $5.6 \times 10^{10}\,\mathrm{M_\odot}$ and $157\,\mathrm{km\,s^{-1}}$, respectively. The R_e and Sérsic index values span the ranges $\sim(0.5$–$40)\,\mathrm{kpc}$ and $\sim 2 - 10$, with medians of $3.2\,\mathrm{kpc}$ and 6.5.

4.2 A test-bench for EG

ETGs are the best candidates to test Verlinde's model, since they are the objects which approach the approximations made by Verlinde (spherical symmetry and isolation) and can be found in large numbers in local environments and higher redshift.

ETGs can have a wide range of shapes and in particular, the axis ratios of the SPIDER galaxies have $q \gtrsim 0.2$, with a distribution

which is peaked at $q \sim 0.75$, with a median of 0.69. If we limit the analysis to the roundest galaxies, e.g. imposing $q > 0.6$, then 2661 out of 4032 are left and the median axis ratio is $q = 0.77$. The environment of ETGs in the SPIDER sample is characterized by a friends-of-friends catalogue of 8083 groups (Berlind et al. 2006; Lopes et al. 2009), classifying galaxies as either group members, field galaxies or unclassified. We select the sample of 1163 field galaxies. See La Barbera et al. (2010b) for further details. The galaxy sample is left with 750 objects, after both the criteria are applied.

In Tortora et al. (2012) we have found that the impact of the galaxy ellipticity and environment on the DM fractions is negligible. A similar result is found in Tortora et al. (2013), fixing the DM profile as discussed in Section 3.1, and finding that IMF is only negligibly affected. These results further support our choice of retaining the whole sample in our EG analysis. We will also demonstrate that the results for EG remain unchanged if only isolated and rounder galaxies are considered.

5 ANALYSIS AND RESULTS

We derive the dynamical (i.e. total) mass distribution of ETGs by solving the spherical isotropic Jeans equations for the three cases of EG, standard DM models and MOND (see 2.2). A given model for the mass profile is fitted to σ_{Ap} for SPIDER.[4] In a Newtonian framework, two-component mass models, describing baryons and DM, are adopted. With MOND, a model for baryons is adopted and equations are modified to account for the change of the force law, as discussed in Section 2.2 (Tortora et al. 2014c).

We assume that gas contributes negligibly to the mass profile, i.e. $M_b(r) = M_\star(r)$ (Courteau et al. 2014; Li et al. 2017). Thus, the baryons are made up by only stars, whose surface brightness is modelled by a Sérsic profile. The shape parameter n and effective radius of the Sérsic laws are those obtained by fitting galaxy images in *K* band (see Section 4). The light distribution is converted into stellar mass by means of a constant stellar M/L ratio, $\Upsilon_\star$, which is a free-fitting parameter. We assume negligible gradients in stellar populations (Tortora et al. 2011) and IMF (Martín-Navarro et al. 2015; Alton, Smith & Lucey 2017).

In the following section we discuss the results of the paper. We will first set constraints on the present-day Hubble parameter in Section 5.1, then in Section 5.2 we fix H_0 and leave the stellar M/L free to change, investigating the shape of the IMF and finally in Section 5.3 we investigate the impact of the entropy strain.

5.1 H_0 free

Because the value of the H_0 enters in both the distances and the EG formula for DM, it is an interesting exercise to first address what would happen in our modelling when it is taken as a free parameter. For simplicity, we start adopting a universal IMF (Chabrier or Salpeter IMF). Then, following the binning procedure in Tortora et al. (2013) and described in Section 3 and adopted in particular for the MOND models, we have created 'average' galaxies by dividing our sample into nine σ_e-bins for which we compute median values and 1σ scatter of all the stellar parameters relevant for our Jeans modelling. Then, fixing the IMF, we perform a joint analysis of the nine 'average' galaxies and determine the best-fitting

---

[3] http://www.sdss.org, http://www.ukidss.org

[4] We use the dynamical procedure described in Tortora et al. (2009) and Tortora et al. (2014a), no seeing correction is adopted.
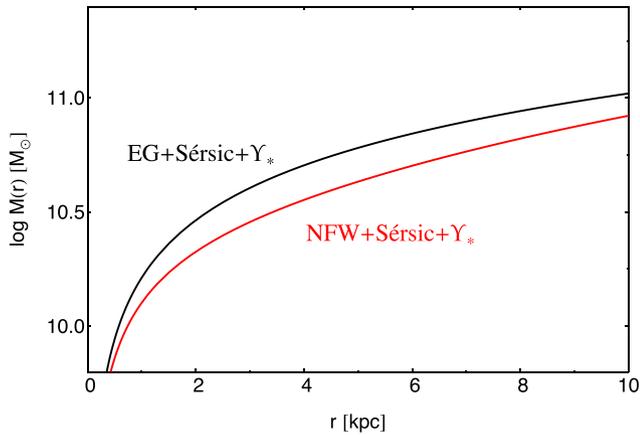
Figure 1. Total mass profile for EG (black line) and our NFW model (red line). We set the parameters to the median values of the sample: $R_e = 3.2$ kpc, $n = 6.5$, the redshift to the SPIDER average value ($z = 0.08$) and $M_\star = 5.6 \times 10^{10}$ M$_\odot$, assuming a Chabrier IMF. The NFW profile is set by fixing M_{vir} and c_{vir} as discussed at the beginning of Section 3.

value of H_0 by minimizing a suitable 'cumulative' χ^2 function $\chi^2 = \sum (\sigma_J - \sigma_{Ap})^2 / \delta\sigma^2$, with σ_J the theoretical σ from the Jeans equation and $\delta\sigma$ the error. In the minimized χ^2, stellar masses, effective radii and R_{Ap}, as well as equation (4), depend on H_0. Finally, note that, with respect to the analysis made to constrain the a_0 in MOND in Tortora et al. (2014c), in this case we are assuming that a_0 explicitly depends on H_0, which means that H_0 cannot vary in terms of galaxy parameters, but has to be universal, since it is a constant of the theory.

We find that in order to match the velocity dispersions of the galaxies in our sample with Verlinde's model, we need a well-fitted $H_0 = 76$ km s^{-1} Mpc^{-1}, if a Chabrier IMF is adopted. Assuming a Salpeter IMF yields $H_0 = 138$ km s^{-1} Mpc^{-1}. Following the discussions in Section 2.2, if we assume that (a) the present-day Hubble parameter has to be consistent with predictions from cosmological probes (e.g. Supernovae Ia or OHD observations); and (b) equation (4) is valid, then, on average, a Chabrier-like IMF would work for our sample of galaxies (see Section 2.2). For the range of velocity dispersions of our sample, this result is consistent with stellar populations and independent estimates, as we will show in the next section.

5.2 IMF free

In the rest of this section we adopt a value of the present day Hubble parameter of $H_0 = 75$ km s^{-1} Mpc^{-1}, consistent with local Universe measurements (e.g. Riess et al. 1998; Jimenez et al. 2003; Percival et al. 2010; Komatsu et al. 2011; Zhang et al. 2014). It is the same used for all the results based on DM models and is consistent with a_0 adopted for the MOND models.

Fig. 1 shows a typical mass profile for EG and our reference DM-based model (i.e. the NFW+baryons), for an example mock galaxy, setting the Sérsic parameters and stellar mass to the median values of the datasample and assuming a Chabrier IMF. The total mass from EG gravity (i.e. the sum of 'apparent' DM and stellar mass) is a factor ∼1.4 larger than the total mass derived from the DM-based NFW model, if we consider the mass profile within R_e. To match the two profiles requires a $\Upsilon_\star$ value in EG smaller of a factor ∼1.5

with respect to a standard DM-based model, or equivalently a $\Upsilon_\star$ value in the reference DM-based model of a factor ∼1.5 larger.

To quantify the ability of EG to fit the data, we discuss the mismatch parameter defined as $\delta_{IMF} \equiv \Upsilon_\star / \Upsilon_{\star Chab}$, where $\Upsilon_\star^{Chab}$ is the M/L obtained by fitting colours with stellar population models having a Chabrier IMF. In Fig. 2 we present δ_{IMF} as a function of effective velocity dispersion σ_e. We find that for EG the values of δ_{IMF} are positively correlated with σ_e, obtaining lower values at the lowest-σ_e (i.e. $\delta_{IMF} \sim 0.7$) and higher values (i.e. $\delta_{IMF} \sim 1.6$) in the galaxies with the highest σ_e; on average $\delta_{IMF} = 0.96$.

Below, we discuss the results shown in Fig. 2 in more details, contrasting the values of δ_{IMF} for EG, with the values found for DM-based, MOND and stellar populations models, and we investigate the impact of various assumptions.

(i) **Panel (a).** In panel (a), the grey shaded region shows the range of the results assuming a wide set of DM-based models, presented in Section 3.1. These results are bracketed by the Burkert profile, producing at fixed σ_e the largest values of δ_{IMF}, and the AC–NFW model, which produces the smallest values of $\Upsilon_\star$ and δ_{IMF}. The red line is the result for our reference NFW profile (Tortora et al. 2013). On average, the δ_{IMF} from EGs are ∼1.3 times smaller than the values for the reference NFW profile.[5] EG models are consistent with DM-based models adopting an AC–NFW.

(ii) **Panel (b).** The EG results are plotted against the results from MOND in panel (b). The cyan region is bracketed by the results for the two standard MOND interpolating functions adopted. The blue line adopts the interpolation function determined in McGaugh et al. (2016) using the rotation curves of the most up-to-date sample of spiral galaxies. The inferred values of δ_{IMF} from EGs are ∼1.4 times smaller than that predicted by MOND.

These results with respect to DM-based and MOND models are consistent with what is found for the bulge components (but not for the discs) in the sample of spiral galaxies in Lelli et al. (2017). Even larger with respect to typical $\Upsilon_\star$ values are found for dwarf spheroidals (Diez-Tejedor et al. 2016). This is expected if we look at the typical baryonic accelerations found in the three different types of galactic objects. Spiral galaxies studied by Lelli et al. (2017) and ETGs studied in the present paper are characterized by similar baryonic accelerations: spirals span the range $\sim 10^{-11.5} - 10^{-9}$ m s^{-2}, while for ETGs the typical accelerations spans $\sim 10^{-11} - 10^{-8.5}$ m s^{-2}. This results in similar values for the fitted $\Upsilon_\star$. While in the deep MOND regime experienced by dwarf spheroidals in Diez-Tejedor et al. (2016), with low accelerations ($\lesssim 10^{-12}$ ms^{-2}), the excess mass is larger. In this case MOND requires values of $\Upsilon_\star$ that are ∼2.5 times greater than those from Verlinde's EG.

(iii) **Panel (c).** In panel (c) of Fig. 2 we present the two best results from gravity-sensitive features determined from stacked SPIDER spectra (La Barbera et al. 2013), assuming a two-slope IMF and adopting two simple stellar population (SSP) models with the same IMF but different ages and metallicities (solid orange line) and two SSP models with free ages and metallicities, including, as further free parameters, the abundances of calcium, sodium and titanium (dashed orange line). The EG results agree with these estimates, which are independent from either DM or gravity arguments,

---

[5] Note that here the factor ∼1.3 is determined solving the Jeans equation and is relative to the aperture of the SDSS fibre. Instead, the ∼1.5 factor discussed at the beginning of this section is obtained finding the best match between the two mass profiles in Fig. 1, within R_e ($> R_{Ap}$).
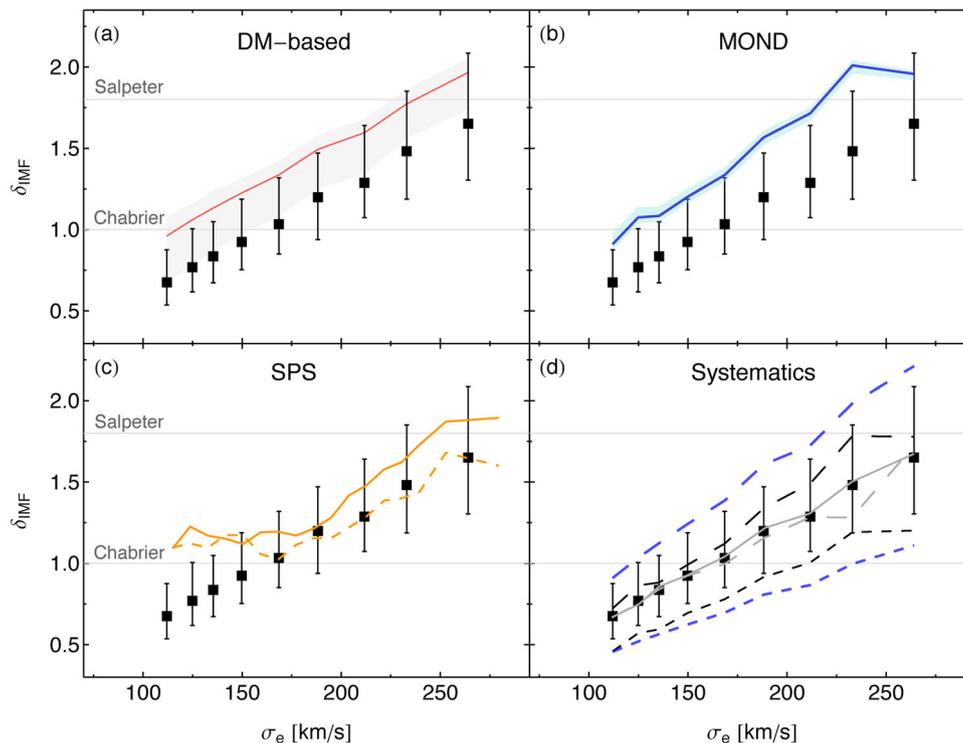
Figure 2. IMF mismatch parameter, δ_{IMF}, for the SPIDER ETGs, as a function of effective velocity dispersion, σ_e. Horizontal lines show the reference values for Chabrier (bottom) and Salpeter (1955) (top) IMF. Black squares and error bars are median and 25–75th percentile trends for EG results. Comparison with other models (DM- and MOND-based) and some systematics are shown in the different panels. Panel (a). Red solid line plots the medians for the fiducial DM-based model (i.e. NFW+Sérsic). Shaded grey region encompasses most of the DM-based models discussed in Tortora et al. (2014a): in particular the region is bracketed by the Burkert and the AC–NFW models. Panel (b). The cyan region is bracketed by the results obtained using the two first MOND interpolating function adopted in this paper. The blue line plots the results using the interpolating function from McGaugh et al. (2016). Panel (c). The orange lines are from the analysis of gravity-sensitive features in SPIDER spectra from La Barbera et al. (2013). Panel (d). For the EG results some systematics are investigated. Long- and short-dashed lines are the medians when highly tangential ($\beta = -1$) and radial ($\beta = 1$) orbits are considered, respectively. Solid and dashed grey lines are for the roundest objects with $q > 0.6$ and for field isolated galaxies, respectively. Short- and long-dashed blue lines are for EG with $H_0 = 50$ and $100\,\mathrm{km\,s^{-1}\,Mpc^{-1}}$.

because they are purely derived from the galaxy spectra and from stellar physics.

(iv) **Panel (d).** The effects of potential sources of systematics are shown in panel (d). First, a possible source of systematics in the EG results is the assumption of isotropic stellar orbits. Thus, we have considered two extreme values of (radially constant) anisotropy parameter β in the Jeans equations (Tortora et al. 2009, 2012, 2016): a tangential anisotropy, $\beta = -1$, and a radial anisotropy, $\beta = 1$, shown in Fig. 2 as long- and short-dashed black lines, respectively. For tangential (radial) anisotropy larger (smaller) δ_{IMF} by a factor ~ 1.1 (~ 1.3) are found with respect to the fiducial isotropic case. Therefore, only if strong radial orbits in ETGs are assumed, EG does not match the results found using DM or MOND and from gravity-sensitive features, producing very low δ_{IMF}, unphysical at low-σ_e, if compared with predictions from synthetic models. However, detailed dynamical modelling in the ETG central regions and simulations find anisotropies to be fairly mild in general, typically in the range $-0.2 \leq \beta \leq +0.3$ (Gerhard et al. 2001; Dekel et al. 2005; Cappellari et al. 2007; Xu et al. 2017). If similar anisotropies would be found within the EG framework, then, the impact on the inferred δ_{IMF} values would be negligible.

We have investigated how the assumption of spherical symmetry and isolation of the galaxies affect our results and whether the sample of galaxies are, on average, sufficient round and far from

companions in order to be considered a proper test-bench for EG (see also Section 2.2). We first restricted the analysis to SPIDER galaxies with K-band axial ratio $q > 0.6$ (see grey solid line in Fig. 2), in order to limit to the rounder galaxies. This subsample consists of 2661 galaxies. The overall results are practically unchanged. Similarly, we found a negligible impact if we limit ourselves to the 1163 field galaxies (grey dashed line in Fig. 2). Consequently, the results are unchanged if we combine these two constraints, limiting the analysis to a sample of 750 isolated and rather round galaxies. As for EG, this small impact of the elliptical shape and of the environment was already verified in our previous analysis (e.g. Tortora et al. 2012; Tortora et al. 2013).

In Section 5.1 we have determined the best-fitting H_0 in EG for a fixed Chabrier and Salpeter IMF. Next we study the impact of different values of H_0 on the inferred values of δ_{IMF}. Although unrealistic, we will adopt two extreme values $H_0 = 50$ and $100\,\mathrm{km\,s^{-1}\,Mpc^{-1}}$. The results are shown in Fig. 2 as short- (long-)dashed blue lines, respectively, with smaller (larger) δ_{IMF} by a factor ~ 1.5 (~ 1.3) with respect to the fiducial case. H_0 values of $\sim 50\,\mathrm{km\,s^{-1}\,Mpc^{-1}}$ would be problematic for Verlinde's EG model yielding very low stellar M/L values, which particularly at low σ would be at odds with predictions from spectral synthesis and independent literature (e.g. La Barbera et al. 2013). We also analysed how these H_0 values impact MOND results, by updating the adopted a_0 and distances with the

new H_0 values. We find similar changes in δ_{IMF}, which will leave unaltered the relative discrepancy between the δ_{IMF} values from EG and MOND.

In first approximation, we notice that if we would account for small residual gas content, then the values of $\Upsilon_\star$ decrease for all the results discussed in this section, potentially leaving unaffected the difference between the different models adopted. However, the analysis of gas contribution could be more complicated than this simple picture, since it will follow a different distribution than stars, potentially impacting the total mass in EG and other models in a different way.

5.3 Entropy strain

Following Verlinde (2017) and all the subsequent literature, we adopted the equality in equation (1). As we discussed in Section 2.2, this is only an assumption. There is no particular motivation to make this assumption.

In Section 5.1, since the acceleration scale is a constant in the EG proposition, we performed a joint analysis of our galaxies considering a_0 to be universal. However, the Hubble parameter in EG, and thus a_0, might be also thought to enclose the information about the elastic medium deformation if the principal strain does not take its maximal value. We will investigate the case when the equality is not valid, introducing a further dimensionless parameter ν_{el} in Verlinde's model, by converting equation (1) in

$$\int_0^r \varepsilon_{\text{DM}}^2(r')A(r')\mathrm{d}r' = \nu_{\text{el}}(r)^2\, V_{M_b}(r). \tag{8}$$

The parameter ν_{el} probes Verlinde's hypothesis of maximum response to the entropy displacement, determining how the elastic medium is responding to baryonic matter. If we consider the inequality in Verlinde's formula, then to a fixed amount of baryons will correspond a smaller ϵ_{DM} and M_{DM}.

We adopt $H_0 = 75\,\text{km}\,\text{s}^{-1}\,\text{Mpc}^{-1}$ and assume a Chabrier IMF. Looked at its face value, ν_{el} acts similarly to δ_{IMF}, although it has a very different meaning, being related to the intrinsic properties of the medium, more than to the gas condensation properties and IMF settling. Thus, velocity dispersions for all the SPIDER galaxies can be reproduced if the parameter ν_{el} varies with σ_e, determining a different change of entropy displacement in terms of the baryon mass. In fact, ϵ_{DM} takes its maximal value at lower masses/σ_e, and is smaller, for larger ν_{el} in equation (8), when larger masses/σ_e galaxies are considered.

Finally, we assume that the IMF is non-universal as found in Section 5.2, and we infer the ν_{el} which matches the typical DM-based, MOND and stellar population results in the literature. The comparison with the results from gravity-sensitive features is good, suggesting that the effective model of Verlinde, and in particular the assumption about equality in equation (1) might be warranted. To recover the results from our reference DM-based model or MOND a value of $\nu_{\text{el}} \sim 1.15 - 1.20$ is found.

6 CONCLUSIONS

We have studied the emergent gravity framework from Verlinde (2017) using the central dynamics of a sample of local massive field and round ETGs. ETGs represent an excellent test-bench of EG because they approximate nearly spherical systems and can also be found in more isolated environments. Under a set of clear stated assumptions (i.e. maximum entropy strain), we show that EG can

reproduce the observed kinematics in the central regions of ETGs, predicting stellar M/L ratios, $\Upsilon_\star$, similar to what is found in spiral galaxies (Hees et al. 2017; Lelli et al. 2017). For EG, to match the central velocity dispersion in ETGs, $\Upsilon_\star$ needs to be non-universal and increasing in values from below a Chabrier to a Salpeter IMF, with increasing stellar velocity dispersion σ_e, and comparable with stellar population studies (see Section 5 for details). However EG produces lower values of $\Upsilon_\star$, if compared with independent frameworks (on average $0.96 \times \Upsilon_{\star\text{Chab}}$, and $0.7 \times \Upsilon_{\star\text{Chab}}$ in the lowest-σ_e systems). This is similar to results found recently by Lelli et al. (2017) for the bulge components in a sample of spiral galaxies. Those authors conclude that EG can be qualitatively consistent with rotation velocity curves and the radial acceleration relation in spiral galaxies, only if we decrease the values of $\Upsilon_\star$. Although these values are lower than MOND predictions and our reference NFW+Sérsic model, the agreement with the $\Upsilon_\star$ derived from gravity-sensitive features in SPIDER spectra or adiabatically contracted DM halo models is quite good (La Barbera et al. 2013).

Thus, the main conclusion of this paper is that EG, DM-based models in a Newtonian framework and MOND do reproduce the central dynamics of ETGs and none of them can be excluded or favoured.

However, in EG, observations can only put a lower bound on the apparent DM (M_{DM}) and acceleration (a_0). Following Verlinde (2017) and the recent literature on the subject, we assumed that the entropy strain ε_{DM} takes its maximal value, a hypothesis which can be also incorrect. If we consider the inequality in the Verlinde's formula (equation 1), then to a given baryonic mass of the galaxy, a lower amount of apparent DM is predicted. If we assume that IMF and H_0 are given, then the entropy strain ϵ_{DM} has to be maximal for galaxies with $\sigma \sim 100\,\text{km}\,\text{s}^{-1}$ and smaller for more massive galaxies. Moreover, if we assume that the strain is not maximal, e.g. ~ 1.2 times smaller, then the central dynamics in ETGs can only be reproduced with a higher stellar M/L ratio.

More detailed analysis is needed to study the entropy strain, to better understand the properties of the medium and the reaction to matter displacement. We plan to further investigate the radial mass density gradients, which can help to discriminate between EG and other frameworks. In addition, an alternative probe is provided by ETG strong gravitational lenses, in particular Einstein rings which are known to have round potentials, which through the measure of the arc radius and of the central dynamics of the lens, allow to determine the lens mass, providing more stringent constraints on the mass profiles and the mass density gradients (e.g. Barnabè et al. 2009, 2011; Treu et al. 2010). It would also be interesting to study samples of galaxies with extended (in radius) kinematical data sets, such as Planetary Nebulae and Globular Clusters. With such galaxies, it is possible to probe the mass distribution in the external regions, where DM effects should be dominant (e.g. Coccato et al. 2009; Napolitano et al. 2009, 2011; Pota et al. 2013, 2015; Alabi et al. 2016). We plan to test the EG formalism with these data sets, probing the apparent mass in equation (4) beyond the effective radius, where the uncertainties in the stellar mass are less relevant and the gas would contribute more to EG.

REFERENCES

Alabi A. B. et al., 2016, MNRAS, 460, 3838

Alton P. D., Smith R. J., Lucey J. R., 2017, MNRAS, 468, 1594

Angus G. W., 2008, MNRAS, 387, 1481

Barnabè M., Czoske O., Koopmans L. V. E., Treu T., Bolton A. S., Gavazzi R., 2009, MNRAS, 399, 21

Barnabè M., Czoske O., Koopmans L. V. E., Treu T., Bolton A. S., 2011, MNRAS, 415, 2215

Barnabè M., Spiniello C., Koopmans L. V. E., Trager S. C., Czoske O., Treu T., 2013, MNRAS, 436, 253

Begeman K. G., Broeils A. H., Sanders R. H., 1991, MNRAS, 249, 523

Berlind A. A. et al., 2006, ApJS, 167, 1

Binney J., Tremaine S., 1987, Galactic dynamics. Princeton Univ. Press, Princeton, NJ

Blumenthal G. R., Faber S. M., Flores R., Primack J. R., 1986, ApJ, 301, 27

Bosma A., 1978, PhD thesis, Univ. Groningen

Brouwer M. M. et al., 2017, MNRAS, 466, 2547

Bruzual G., Charlot S., 2003, MNRAS, 344, 1000

Burkert A., 1995, ApJ, 447, L25

Cappellari M. et al., 2006, MNRAS, 366, 1126

Cappellari M. et al., 2007, MNRAS, 379, 418

Cappellari M. et al., 2012, Nature, 484, 485

Cappellari M. et al., 2013, MNRAS, 432, 1862

Cardone V. F., Angus G., Diaferio A., Tortora C., Molinaro R., 2011, MNRAS, 412, 2617

Carvalho F. C., Santos E. M., Alcaniz J. S., Santos J., 2008, J. Cosmology Astropart. Phys., 9, 008

Chabrier G., 2003, PASP, 115, 763

Ciotti L., 1991, A&A, 249, 99

Coccato L. et al., 2009, MNRAS, 394, 1249

Conroy C., van Dokkum P. G., 2012, ApJ, 760, 71

Corsini E. M., Wegner G. A., Thomas J., Saglia R. P., Bender R., 2017, MNRAS, 466, 974

Courteau S. et al., 2014, Rev. Mod. Phys., 86, 47

de Vaucouleurs G., 1948, Ann. Astrophysique, 11, 247

Dekel A., Stoehr F., Mamon G. A., Cox T. J., Novak G. S., Primack J. R., 2005, Nature, 437, 707

Diez-Tejedor A., Gonzalez-Morales A. X., Niz G., 2016, preprint (arXiv:1612.06282)

Dutton A. A., Macciò A. V., Mendel J. T., Simard L., 2013, MNRAS, 432, 2496

Ettori S., Ghirardini V., Eckert D., Dubath F., Pointecouteau E., 2017, MNRAS, 470, L29

Famaey B., Binney J., 2005, MNRAS, 363, 603

Farooq O., Ranjeet Madiyar F., Crandall S., Ratra B., 2017, ApJ, 835, 26

Ferreras I., Mavromatos N. E., Sakellariadou M., Yusaf M. F., 2012, Phys. Rev. D, 86, 083507

Ferreras I., La Barbera F., de la Rosa I. G., Vazdekis A., de Carvalho R. R., Falcón-Barroso J., Ricciardelli E., 2013, MNRAS, 429, L15

Fukugita M., Hogan C. J., Peebles P. J. E., 1998, ApJ, 503, 518

Gerhard O., Kronawitter A., Saglia R. P., Bender R., 2001, AJ, 121, 1936

Gnedin O. Y., Kravtsov A. V., Klypin A. A., Nagai D., 2004, ApJ, 616, 16

Goudfrooij P., Kruijssen J. M. D., 2013, ApJ, 762, 107

Goudfrooij P., Kruijssen J. M. D., 2014, ApJ, 780, 43

Hees A., Famaey B., Bertone G., 2017, Phys. Rev. D, 95, 064019

Hilz M., Naab T., Ostriker J. P., 2013, MNRAS, 429, 2924

Jacobson T., 1995, Phys. Rev. Lett., 75, 1260

Jimenez R., Verde L., Treu T., Stern D., 2003, ApJ, 593, 622

Komatsu E. et al., 2011, ApJS, 192, 18

Kroupa P., 2001, MNRAS, 322, 231

La Barbera F., de Carvalho R. R., Kohl-Moreira J. L., Soares-Santos M., Capaccioli M., Santos R., Sant'Anna N., 2008, PASP, 120, 681

La Barbera F., de Carvalho R. R., de La Rosa I. G., Lopes P. A. A., Kohl-Moreira J. L., Capelato H. V., 2010a, MNRAS, 408, 1313

La Barbera F., Lopes P. A. A., de Carvalho R. R., de La Rosa I. G., Berlind A. A., 2010b, MNRAS, 408, 1361

La Barbera F., Ferreras I., Vazdekis A. de la Rosa I. G., de Carvalho R. R., Trevisan M., Falcón-Barroso J., Ricciardelli E., 2013, MNRAS, 433, 3017

Lelli F., McGaugh S. S., Schombert J. M., 2017, MNRAS, 468, L68

Li H. et al., 2017, ApJ, 838, 77

Lopes P. A. A., de Carvalho R. R., Kohl-Moreira J. L., Jones C., 2009, MNRAS, 392, 135

Lyubenova M. et al., 2016, MNRAS, 463, 3220

Macciò A. V., Dutton A. A., van den Bosch F. C., 2008, MNRAS, 391, 1940

Martín-Navarro I., Barbera F. L., Vazdekis A., Falcón-Barroso J., Ferreras I., 2015, MNRAS, 447, 1033

McDermid R. M. et al., 2014, ApJ, 792, L37

McGaugh S. S., 2012, AJ, 143, 40

McGaugh S. S., Lelli F., Schombert J. M., 2016, Phys. Rev. Lett., 117, 201101

Memola E., Salucci P., Babić A., 2011, A&A, 534, A50

Milgrom M., 1983a, ApJ, 270, 371

Milgrom M., 1983b, ApJ, 270, 365

Milgrom M., 2001, Acta Phys. Pol. B, 32, 3613

Milgrom M., 2012, Phys. Rev. Lett., 109, 131101

Milgrom M., Sanders R. H., 2016, preprint (arXiv:1612.09582)

Moster B. P., Somerville R. S., Maulbetsch C., van den Bosch F. C., Macciò A. V., Naab T., Oser L., 2010, ApJ, 710, 903

Napolitano N. R. et al., 2009, MNRAS, 393, 329

Napolitano N. R., Romanowsky A. J., Tortora C., 2010, MNRAS, 405, 2351

Napolitano N. R. et al., 2011, MNRAS, 411, 2035

Navarro J. F., Frenk C. S., White S. D. M., 1996, ApJ, 462, 563

Navarro J. F., Frenk C. S., White S. D. M., 1997, ApJ, 490, 493

Nieuwenhuizen T. M., 2017, Fortschr. Phys., 65, 201600050

Padmanabhan T., 2004, Int. J. Mod. Phys. D, 13, 2293

Padmanabhan T., 2010, Rep. Prog. Phys., 73, 046901

Pardo K., 2017, JCAP, preprint (arXiv:1706.00785)

Percival W. J. et al., 2010, MNRAS, 401, 2148

Pota V. et al., 2013, MNRAS, 428, 389

Pota V. et al., 2015, MNRAS, 450, 3345

Riess A. G. et al., 1998, AJ, 116, 1009

Salpeter E. E., 1955, ApJ, 121, 161

Salucci P., Burkert A., 2000, ApJ, 537, L9

Sanders R. H., 2014, MNRAS, 439, 1781

Sanders R. H., McGaugh S. S., 2002, ARA&A, 40, 263

Shu Y. et al., 2015, ApJ, 803, 71

Sindoni L., 2012, SIGMA, 8, 027

Sonnenfeld A., Nipoti C., Treu T., 2017, MNRAS, 465, 2397

Spiniello C., Trager S. C., Koopmans L. V. E., Chen Y. P., 2012, ApJ, 753, L32

Spiniello C., Barnabè M., Koopmans L. V. E., Trager S. C., 2015, MNRAS, 452, L21

Swindle R., Gal R. R., La Barbera F., de Carvalho R. R., 2011, AJ, 142, 118

Thomas J. et al., 2011, MNRAS, 415, 545

Tortora C., Napolitano N. R., Romanowsky A. J., Capaccioli M., Covone G., 2009, MNRAS, 396, 1132

Tortora C., Napolitano N. R., Romanowsky A. J., Jetzer P., Cardone V. F., Capaccioli M., 2011, MNRAS, 418, 1557

Tortora C., La Barbera F., Napolitano N. R., de Carvalho R. R., Romanowsky A. J., 2012, MNRAS, 425, 577

Tortora C., Romanowsky A. J., Napolitano N. R., 2013, ApJ, 765, 8

Tortora C., La Barbera F., Napolitano N. R., Romanowsky A. J., Ferreras I., de Carvalho R. R., 2014a, MNRAS, 445, 115

Tortora C., Napolitano N. R., Saglia R. P., Romanowsky A. J., Covone G., Capaccioli M., 2014b, MNRAS, 445, 162

Tortora C., Romanowsky A. J., Cardone V. F., Napolitano N. R., Jetzer P., 2014c, MNRAS, 438, L46

Tortora C., La Barbera F., Napolitano N. R., 2016, MNRAS, 455, 308

Tortora C. et al., 2017, MNRAS, preprint (arXiv:1709.03542)

Treu T., Auger M. W., Koopmans L. V. E., Gavazzi R., Marshall P. J., Bolton A. S., 2010, ApJ, 709, 1195

Tully R. B., Fisher J. R., 1977, A&A, 54, 661

van Dokkum P. G., Conroy C., 2010, Nature, 468, 940

Verlinde E., 2011, J. High Energy Phys., 4, 29

Verlinde E. P., 2017, SciPost Phys., 2, 016

Vulcani B. et al., 2011, MNRAS, 413, 921

Wegner G. A., Corsini E. M., Thomas J., Saglia R. P., Bender R., Pu S. B., 2012, AJ, 144, 78

Weidner C., Ferreras I., Vazdekis A., La Barbera F., 2013, MNRAS, 435, 2274

Xu D., Springel V., Sluse D., Schneider P., Sonnenfeld A., Nelson D., Vogelsberger M., Hernquist L., 2017, MNRAS, 469, 1824

Zhang C., Zhang H., Yuan S., Liu S., Zhang T.-J., Sun Y.-C., 2014, Res. Astron. Astrophys., 14, 1221

This paper has been typeset from a TEX/LATEX file prepared by the author.